

Anthropogenic and biophysical contributions to increasing atmospheric CO₂ growth rate and airborne fraction

M. R. Raupach¹, J. G. Canadell¹, and C. Le Quéré^{2,3}

¹Global Carbon Project, CSIRO Marine and Atmospheric Research, Canberra, Australia

²School of Environmental Sciences, University of East Anglia, Norwich, UK

³British Antarctic Survey, Cambridge, UK

Received: 2 June 2008 – Published in Biogeosciences Discuss.: 11 July 2008

Revised: 2 October 2008 – Accepted: 4 October 2008 – Published: 28 November 2008

Abstract. We quantify the relative roles of natural and anthropogenic influences on the growth rate of atmospheric CO₂ and the CO₂ airborne fraction, considering both interdecadal trends and interannual variability. A combined ENSO-Volcanic Index (EVI) relates most (~75%) of the interannual variability in CO₂ growth rate to the El-Niño-Southern-Oscillation (ENSO) climate mode and volcanic activity. Analysis of several CO₂ data sets with removal of the EVI-correlated component confirms a previous finding of a detectable increasing trend in CO₂ airborne fraction (defined using total anthropogenic emissions including fossil fuels and land use change) over the period 1959–2006, at a proportional growth rate 0.24% y⁻¹ with probability ~0.9 of a positive trend. This implies that the atmospheric CO₂ growth rate increased slightly faster than total anthropogenic CO₂ emissions. To assess the combined roles of the biophysical and anthropogenic drivers of atmospheric CO₂ growth, the increase in the CO₂ growth rate (1.9% y⁻¹ over 1959–2006) is expressed as the sum of the growth rates of four global driving factors: population (contributing +1.7% y⁻¹); per capita income (+1.8% y⁻¹); the total carbon intensity of the global economy (–1.7% y⁻¹); and airborne fraction (averaging +0.2% y⁻¹ with strong interannual variability). The first three of these factors, the anthropogenic drivers, have therefore dominated the last, biophysical driver as contributors to accelerating CO₂ growth. Together, the recent (post-2000) increase in growth of per capita income and decline in the negative growth (improvement) in the carbon intensity of the economy will drive a significant further acceleration in the CO₂ growth rate over coming decades, unless these recent trends reverse.

1 Introduction

Atmospheric CO₂ concentrations have risen over the last 200 years at an accelerating rate, in response to increasing anthropogenic CO₂ emissions. The resulting CO₂ disequilibrium has led to uptake of CO₂ from the atmosphere by land and ocean CO₂ sinks, which currently remove over half of all anthropogenic emissions and thereby provide a strong negative (stabilising) feedback on the carbon-climate system (Gruber et al., 2004; Sabine et al., 2004). The CO₂ airborne fraction (the fraction of total emissions from fossil fuels and land use change accumulating in the atmosphere) has averaged 0.43 since 1959, but has increased through that period at about 0.2% y⁻¹ (Canadell et al., 2007). These interdecadal trends in CO₂ growth rate and the airborne fraction are the outcome of a race between two groups of forcing factors: the social, economic and technical drivers of anthropogenic emissions (including population, wealth and the carbon intensity of the economy), and the biophysical drivers of trends in land and ocean sinks.

The CO₂ growth rate also varies strongly at interannual (~1 to ~10 y) time scales, through mainly biophysical mechanisms. Fluctuations in CO₂ growth rate correlate with the El-Niño-Southern-Oscillation (ENSO) climate mode (Keeling and Revelle, 1985; Keeling et al., 1995; Jones and Cox, 2005), because the terrestrial carbon balance in tropical regions is tilted from uptake to release of CO₂ during dry, warm El-Niño events (Zeng et al., 2005; Knorr et al., 2005). Volcanic events are also significant: the CO₂ growth rate decreased for several years after the eruption of Mt. Pinatubo in June 1991 (Jones et al., 2001), probably because of increased net carbon uptake by terrestrial ecosystems due to higher diffuse solar radiation (Gu et al., 2003) and cooler temperatures (Jones and Cox, 2001) caused by volcanic aerosols.



Correspondence to: M. R. Raupach
(michael.raupach@csiro.au)

This interannual variability in the CO₂ growth rate is important for two reasons: it indicates mechanisms that govern the land and ocean CO₂ sinks, and it masks important longer-term trends in the CO₂ growth rate with strong variability at higher frequencies.

In this paper we investigate the combined anthropogenic and biophysical drivers of atmospheric CO₂ growth rates, with three aims. First, we obtain a simple quantification of the leverage of ENSO and volcanic signals on global CO₂ sinks at interannual time scales, using a combined ENSO-Volcanic Index (EVI). Second, we analyse observed interdecadal trends in the CO₂ airborne fraction by removing the interannual variability associated with the EVI from several CO₂ records, confirming and extending the preliminary findings of Canadell et al. (2007). Third, we introduce an extended form of the Kaya identity which combines the biophysical and anthropogenic drivers of CO₂ growth, and use it both to diagnose the drivers of past trends and offer some indicative estimates of future CO₂ growth rates.

2 Framework

2.1 Atmospheric CO₂ budget and airborne fraction

The global atmospheric CO₂ budget is written as

$$\begin{aligned} C'_a &= F_E + F_S \\ &= (F_{\text{Fossil}} + F_{\text{LUC}}) + (F_{\text{LandAir}} + F_{\text{OceanAir}}) \end{aligned} \quad (1)$$

where $C_a = v_a[\text{CO}_2]$ is the mass of atmospheric CO₂ (with $[\text{CO}_2]$ the atmospheric CO₂ mole fraction and $v_a = 2.127 \text{ PgC ppm}^{-1}$); $C'_a = dC_a/dt$ is the growth rate of atmospheric CO₂ (with primes denoting time derivatives); F_E is the total anthropogenic CO₂ emission flux including emissions from fossil fuels (F_{Fossil}) and net emissions from land use change (F_{LUC}); and F_S is the total surface-air exchange flux including land-air and ocean-air fluxes (F_{LandAir} and F_{OceanAir}). All fluxes are positive into the atmosphere, so $F_S < 0$ in the current era and the total CO₂ sink is $-F_S$.

The CO₂ airborne fraction, the fraction of emissions accumulating in the atmosphere, has two extant definitions based respectively on total anthropogenic emissions from both fossil fuels and land use change ($F_E = F_{\text{Fossil}} + F_{\text{LUC}}$), and on fossil-fuel emissions only (F_{Fossil}):

$$a_E = C'_a/F_E; \quad a_{\text{Fossil}} = C'_a/F_{\text{Fossil}} \quad (2)$$

where the subscript denotes the normalising flux. The former (a_E) is the “total” airborne fraction, while the latter (a_{Fossil}) has been called the “apparent” airborne fraction (Oeschger et al., 1980; Enting, 2007). Similarly, a sink fraction (the fraction of emissions taken up by land and ocean sinks, $-F_S$) can be defined in two ways as $s_E = -F_S/F_E$ (total) and $s_{\text{Fossil}} = -F_S/F_{\text{Fossil}}$ (apparent). The relationships between the respective airborne and sink fractions are

$$a_E = 1 - s_E; \quad a_{\text{Fossil}} = 1 - s_{\text{Fossil}} + (F_{\text{LUC}}/F_{\text{Fossil}}) \quad (3)$$

The total airborne fraction a_E is preferable in principle to the apparent a_{Fossil} , for two reasons. First, a_E is the ratio of total response of the atmospheric carbon cycle (C'_a) to total forcing (F_E), whereas a_{Fossil} is the ratio of total response (C'_a) to a partial forcing (F_{Fossil}), omitting F_{LUC} . Second (and in consequence), the total airborne and sink fractions add to 1, so trends in a_E are always opposite to trends in s_E and either fraction is a direct measure of the outcome of the combined influences of total emissions and total sinks on the CO₂ growth rate. The apparent airborne and sink fractions do not have this property because the additional forcing from land use change has to be included separately as in Eq. (3). For both reasons a_E is used here as the primary measure of airborne fraction, though results are also given for a_{Fossil} .

Longstanding use of the apparent airborne fraction was originally motivated not from basic considerations but by the methodological problem of lack of knowledge of F_{LUC} . However, the situation has now changed with improved data, especially from satellites. Recent estimates of F_{LUC} have converged on $1.5 \pm 0.5 \text{ PgC y}^{-1}$ for 2000–2006, compared with $F_{\text{Fossil}} \approx 7.6 \pm 0.4$ and $C'_a \approx 4.1 \pm 0.1 \text{ PgC y}^{-1}$ over the same period (Canadell et al., 2007).

The sink fraction ($s_E = -F_S/F_E$) can be split into a land fraction (l_E) and an ocean fraction (o_E):

$$l_E = -F_{\text{LandAir}}/F_E; \quad o_E = -F_{\text{OceanAir}}/F_E \quad (4)$$

The sink fraction is $s_E = l_E + o_E$, and the airborne, land and ocean fractions sum to 1:

$$a_E + l_E + o_E = 1 \quad (5)$$

2.2 Data

We used the following data for the period 1959 to 2006 (see Appendix A for sources and details):

- annual global CO₂ emissions F_{Fossil} and F_{LUC} ;
- monthly CO₂ series with the annual cycle removed, from atmospheric baseline stations at Mauna Loa, Hawaii (MLO) and the South Pole (SPO), together with two estimates of globally averaged CO₂ concentration: the first (GLA) was formed from the average of MLO and SPO, and the second (GLB) consisted of a globally-averaged CO₂ series available from January 1980 onward, augmented with MLO data for 1958–1979;
- five monthly ENSO indices: eastern (Niño3), central (Niño3.4) and western (Niño4) equatorial Pacific sea surface temperatures, the Southern Oscillation Index (SOI), and the Multivariate ENSO Index (MEI);
- the monthly global Volcanic Aerosol Index (VAI);
- global population and Gross Domestic Product by Purchasing Power Parity (GDP-PPP).

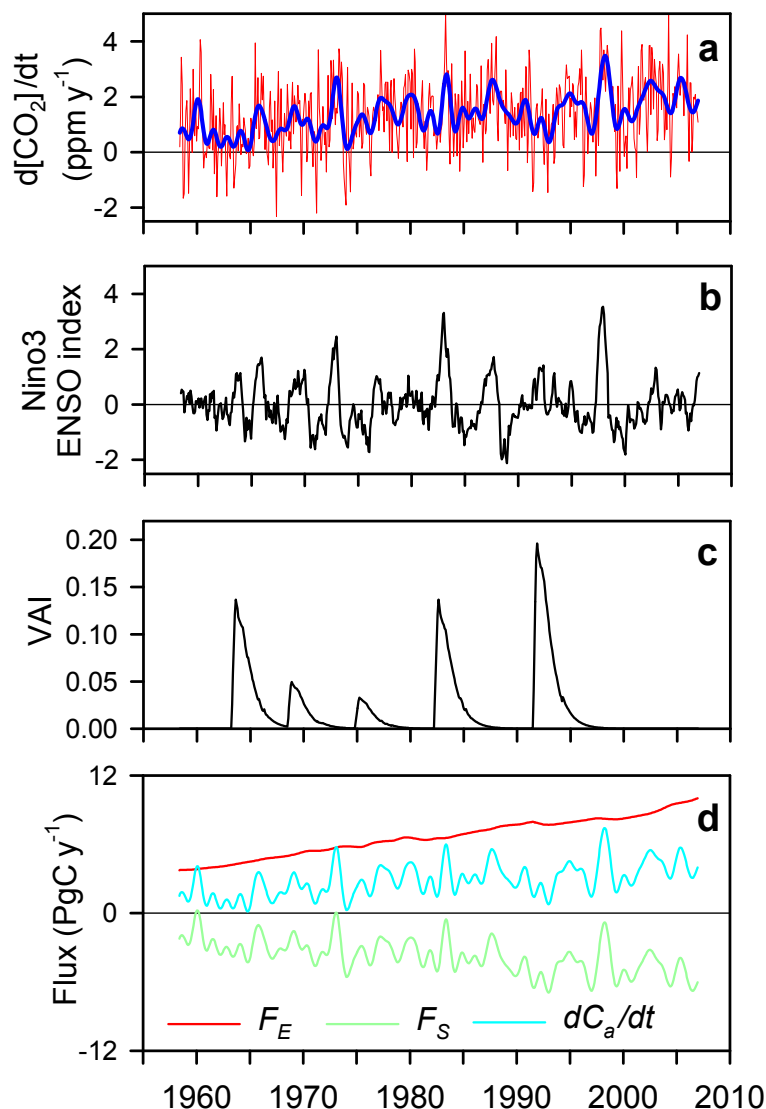


Fig. 1. Monthly time series for (a) CO₂ growth rate C'_a , without and with lowpass filtering ($f_i 0.8 \text{ y}^{-1}$); (b) the Niño3 ENSO index; (c) the VAI; (d) terms in the atmospheric CO₂ budget, $C'_a = F_E + F_S$, with lowpass filtering. The growth rate C'_a is from the GLA series (average of MLO and SPO with annual cycle removed).

The analysis was done at a monthly time step, with slowly varying annual data (emissions, population, GDP-PPP) interpolated to monthly (details in Appendix A).

3 Interannual variability of CO₂ growth rate

3.1 Spectral structure of CO₂ growth and ENSO

Figure 1a, b and c respectively show time series of the CO₂ growth rate C'_a , a typical ENSO index (Niño3) and the VAI. There is much more high-frequency structure in C'_a than in the ENSO index, because point time series of C'_a contain significant high-frequency signal arising from incomplete mixing of air transported from regions with very different CO₂

sources and sinks at the earth surface. In contrast, ENSO indices based on large-area-average ocean temperatures are temporally smoother because of the longer inherent time scales of changes in ocean surface temperatures.

This observation is quantified in Fig. 2, by plotting normalised cumulative spectra and cospectra of the CO₂ growth rate and each of the five ENSO indices (Niño3, Niño3.4, Niño4, SOI, and MEI). Normalised (co)spectra show the fractional contribution to the (co)variance from frequencies less than a given frequency (see Appendix B for details). The spectra (Fig. 2a) reveal much more high-frequency content in C'_a than the ENSO indices, consistent with the above qualitative observation. More significantly, the C'_a -ENSO cospectra (Fig. 2b) show that all of the covariance between C'_a and any

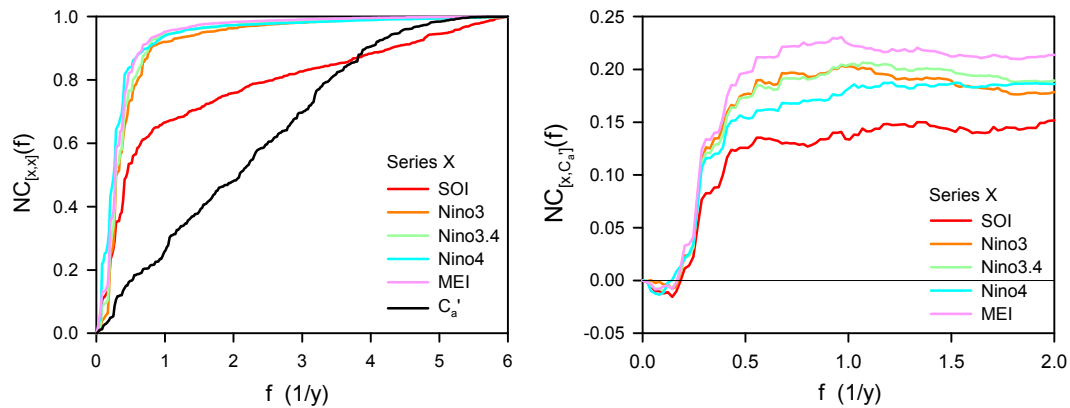


Fig. 2. (Left) normalised cumulative spectra of C'_a (black) and ENSO indices (coloured), showing the total fraction of the variance contributed by frequencies less than f . (Right) normalised cumulative cospectra of C'_a with ENSO indices. Colour code for ENSO indices: SOI (red), Niño3 (orange), Niño3.4 (green), Niño4 (blue), MEI (pink). These results use the GLA (average of MLO and SPO) series for CO₂ growth rate; equivalent results with MLO and SPO series separately are very similar.

of the five ENSO indices is spectrally band-limited to frequencies in a narrow window between ~ 0.2 and $\sim 0.8 \text{ y}^{-1}$ (periods from ~ 5 to $\sim 1.25 \text{ y}$). Spectral components of C'_a and ENSO indices at higher frequencies are uncorrelated and add nothing to the covariance, their only effect being to degrade the correlation by adding high-frequency noise. It is therefore useful to filter out the high-frequency noise for diagnosis of the relationship between ENSO and carbon fluxes. Henceforth all time series are lowpass-filtered with a Fourier-transform filter which removes frequencies $f > 0.8 \text{ y}^{-1}$ or periods < 15 months (Appendix B).

Figure 1d shows the terms in the lowpass-filtered atmospheric CO₂ budget, $C'_a = F_E + F_S$. Lowpass filtering has negligible effect on F_E because it is slowly-varying relative to C'_a . Consequently, the C'_a spectra and C'_a -ENSO cospectra (Fig. 2) are practically indistinguishable from equivalent spectra and cospectra (not shown) constructed with F_S .

3.2 Correlations between surface-air exchange flux, ENSO and volcanic activity

The mechanistic links between ENSO, volcanic activity and the CO₂ budget occur through the total (land plus ocean) surface-air exchange flux $F_S = C'_a - F_E$, rather than through C'_a . Therefore we examine lagged correlations between F_S (rather than C'_a) and ENSO and volcanic indices. The lagged correlation between time series $X(t)$ and $Y(t)$ is

$$\text{Corr}_{[X,Y]}(\tau) = \langle X(t)Y(t+\tau) \rangle / (\sigma_X \sigma_Y) \quad (6)$$

where τ is the time lag, angle brackets denote an average over time t , and σ_X and σ_Y are the standard deviations of X and Y .

Lagged correlations between the five ENSO indices and F_S (Fig. 3, left) confirm the well-known relationship (Keeling and Revelle, 1985; Keeling et al., 1995; Jones and Cox,

2005) between ENSO and CO₂ growth rate. Peak correlations between ENSO and F_S (using C'_a at MLO) depend on the choice of ENSO index, ranging between 0.62 for Niño3 and 0.45 for Niño4. The peak correlation is positive (so positive ENSO index anomalies, corresponding with dry, warm El-Niño events, are associated with positive anomalies in F_S or negative anomalies in the total sink $-F_S$). The peak occurs when F_S lags the ENSO index by 3 ± 1 months.

To include the influences of both ENSO and volcanic activity on CO₂ fluxes and growth rate, we define an ENSO-Volcanic Index (EVI) as the linear combination

$$\text{EVI}(t) = \text{ENSOI}(t-\tau) + \lambda \text{VAI}(t) \quad (7)$$

where ENSOI is an ENSO index normalised to zero mean and unit variance; VAI is the global Volcanic Aerosol Index, a measure of volcanically-induced aerosol optical depth (Ammann et al., 2003); λ is the weight for VAI relative to ENSOI; and τ is the ENSO lag time, a measure of the time for ENSO to affect the CO₂ exchange flux F_S . It is assumed that the VAI affects F_S without time lag. Five alternative versions of the EVI are obtained, corresponding to the five ENSO indices. The EVI depends on two parameters, λ and τ , both of which are well constrained. From Fig. 3 (left) we used $\tau = 3$ months for all ENSO indices, so that the maximum correlation between EVI and F_S occurs near $t = 0$. The weight λ was chosen so that the EVI explains as much as possible of F_S , which occurs when λ takes the value maximising the correlation between EVI and F_S . For all five EVI this is close to $\lambda = -16$, the value used hereafter.

Use of the EVI in place of an ENSO index increases the peak correlations with F_S substantially (Fig. 3, right). With F_S calculated from C'_a at MLO and an EVI defined from Niño3, the peak correlation is 0.75. Figure 4 compares peak correlations between the ENSO indices and F_S , and between the corresponding EVI and F_S , using C'_a at both MLO and

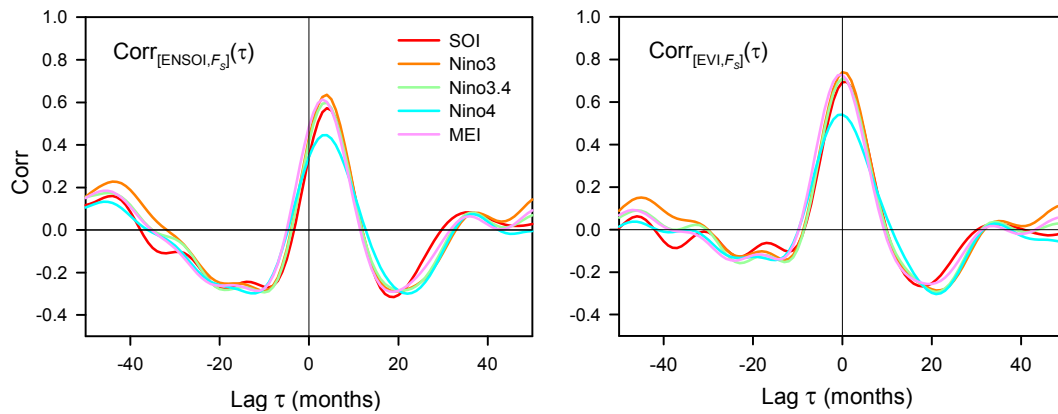


Fig. 3. Lagged cross-correlation functions between (left) ENSO indices and F_S , $\text{Corr}[\text{ENSOI}, F_S](\tau)$, and (right) corresponding ENSO-Volcanic Indices (EVI) and F_S , $\text{Corr}[\text{EVI}, F_S](\tau)$. The surface-air exchange flux $F_S = C'_a - F_E$ was calculated using C'_a from the GLA series (average of MLO and SPO with annual cycle removed). All series are lowpass-filtered ($f_i 0.8 \text{ y}^{-1}$). Colour code for different ENSO indices and corresponding EVI matches Fig. 2.

SPO. Correlations are slightly lower at SPO than MLO, but are still increased by using the EVI rather than corresponding ENSO index. Since λ is negative, a positive anomaly in the VAI component of the EVI is associated with a positive anomaly in the sink $-F_S$ (while a positive anomaly in the ENSO component is associated with negative anomaly in $-F_S$ as noted above).

4 Interdecadal trends in CO₂ airborne fraction

4.1 Initial trend estimate

The total airborne fraction ($a_E = C'_a / F_E = 1 + F_S / F_E$) provides a measure of the relationship between total CO₂ emissions and sinks. We estimated trends in monthly series of a_E inferred from C'_a records from 1959 to 2006. Since a_E is inherently globally aggregated, it is necessary to use estimates of a globally-averaged C'_a . Two estimates were used (see Sect. 2 and Appendix A): from the average of the MLO and SPO CO₂ series with annual cycle removed (denoted GLA), and from a globally-averaged CO₂ series available from 1980 onward, augmented with MLO data before 1980 (denoted GLB).

The trend in a_E was estimated using a stochastic method which accounts for temporal correlation in the time series (see Appendix C for details). The trend is expressed here as a proportional growth rate, defined for a time series $X(t)$ as $r(X) = X' / X$, with units $\% \text{ y}^{-1}$.

The GLA series for 1959–2006 yielded a mean a_E of 0.43 and a proportional growth rate $r(a_E) = 0.24\% \text{ y}^{-1}$ (with 5% and 95% confidence limits -0.18 and $0.64\% \text{ y}^{-1}$ and probability $P = 0.81$ of a positive trend). The result from the GLB series was nearly identical. This result does not provide an unambiguous, statistically robust determination of the trend in a_E .

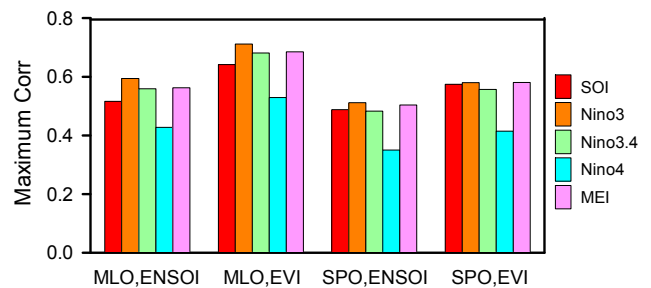


Fig. 4. Maximum lagged correlations between ENSO indices and F_S , and between EVI and F_S , using F_S from CO₂ at MLO and SPO. All series are lowpass-filtered ($f_i 0.8 \text{ y}^{-1}$). Colour code for different ENSO indices and corresponding EVI matches Fig. 2.

4.2 Noise reduction

Detection of trends in a_E can be improved in statistical significance by removing the interannually varying component which is causally linked with ENSO and volcanic activity, using the EVI.

We write an arbitrary time series $X(t)$ as the sum of trend (X^T), mean-annual-cycle (X^C) and anomaly (X^A) components: $X = X^T + X^C + X^A$. The anomaly component is further split as $X^A = X^E + X^U$, where X^U is a noise component uncorrelated with the EVI and X^E is linearly dependent on the EVI. This component is $X^E(t) = \mu \text{EVI}^A(t)$, where μ is the sensitivity of X to the EVI, and use of the anomaly component EVI^A ensures that $X^E(t)$ has zero mean, no trend and no annual cycle. The full decomposition is thus

$$X = X^T + X^C + \mu \text{EVI}^A + X^U \quad (8)$$

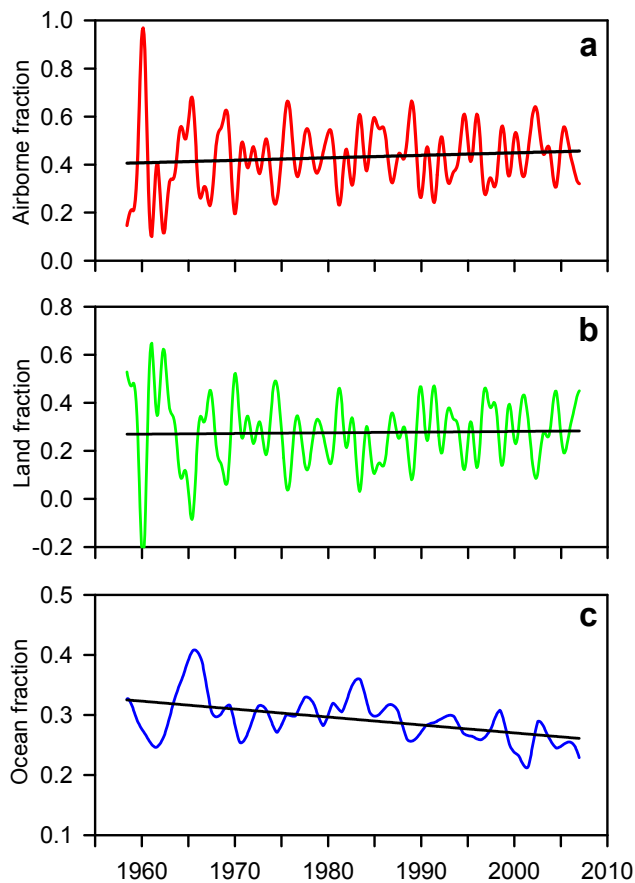


Fig. 5. Monthly time series of airborne fraction (a_E), land fraction (l_E) and ocean fraction (o_E). All series are lowpass filtered ($f; 0.8 \text{ y}^{-1}$) and noise-reduced by removal of the EVI-correlated fluctuating component.

When X is a time series over N monthly time points t_n ($n=1, \dots, N$), the components are given by:

$$\begin{aligned}
 X^T(t_n) &= P(t_n) \\
 X^F(t_n) &= X(t_n) - X^T(t_n) \\
 X^C(t_n) &= \left\langle X^F(t_n) \mid \text{mod}(n, 12) = m \right\rangle \\
 X^A(t_n) &= X^F(t_n) - X^C(t_n)
 \end{aligned} \quad (9)$$

where the trend is defined by fitting a polynomial P to $X(t_n)$, $\langle \bullet \rangle$ denotes an average over the record, and $\langle \bullet \mid \text{condition} \rangle$ denotes a conditional average.

The noise-reduced version of $X(t)$, denoted with a superscript (n), is given by subtracting out the externally-forced components X^C and $X^E = \mu \text{EVI}^A$:

$$\begin{aligned}
 X^{(n)}(t) &= X(t) - X^C(t) - \mu \text{EVI}^A(t) \\
 &= X^T(t) + X^U(t)
 \end{aligned} \quad (10)$$

The trends of the noise-reduced and original series are identical because the components removed have zero mean and no trend, but the variability of the new series is lower, improving the statistical significance of trends.

This decomposition was applied to the CO₂ sink F_S , yielding noise-reduced series $F_S^{(n)}$, $C_a^{(n)} = F_E - F_S^{(n)}$ and airborne fraction $a_E^{(n)} = C_a^{(n)} / F_E$. The sensitivity μ was chosen to minimise the variance of $F_S^U = F_S^A - \mu \text{EVI}^A$, thus placing as much as possible of the anomaly F_S^A into the EVI-correlated component. With lowpass-filtered series F_S and EVI, using an EVI defined from Niño3, the resulting sensitivity is $\mu = 0.9$.

With noise reduction, the GLA series for 1959–2006 yielded a proportional growth rate in total airborne fraction, $r(a_E^{(n)})$, of $0.24\% \text{ y}^{-1}$ (5% and 95% confidence limits -0.04 and $0.50\% \text{ y}^{-1}$; probability $P=0.92$ of a positive trend), around a mean $a_E^{(n)}$ of 0.43 . The result with the GLB series is similar but with a slightly lower P of 0.88 . Noise reduction therefore does not change the mean result from the above initial trend estimate but provides improved statistical reliability, raising P from 0.81 to about 0.9 . This more complete analysis with multiple CO₂ series confirms our earlier result (Canadell et al., 2007) which was derived from the GLB series.

Figure 5 shows the noise-reduced airborne fraction, together with the corresponding noise-reduced land and ocean fractions defined in Eq. (4). The ocean fraction was calculated using a model (Le Quéré et al., 2007) for the time history of the ocean uptake flux (F_{OceanAir}), and the land fraction was calculated as $1 - a_E - o_E$ (Eq. 5). As previously reported (Canadell et al., 2007), there is a highly significant decreasing trend in ocean fraction at $r(o_E) = 0.4 \pm 0.1 \text{ y}^{-1}$ (5% and 95% confidence limits). There is no significant trend in the land fraction. This indicates that the 1959–2006 increase in a_E has been driven mainly by a relative weakening of the ocean sink compared with total emissions F_E . Although the ocean sink has increased in absolute terms, it has not kept pace with growth in total emissions.

We also determined the trend in the apparent airborne fraction (a_{Foss}), even though a_E is the more fundamental carbon-cycle attribute for reasons given in Sect. 2. The proportional growth rate of a_{Foss} for 1959–2006 is small and negative, with $r(a_{\text{Foss}}) \approx -0.2 \pm 0.2\% \text{ y}^{-1}$ around a mean of 0.57 . The different trends in a_E and a_{Foss} are easily understandable by noting that $r(a_{\text{Foss}})$ is the sum of $r(a_E)$ and the growth rate $r(a_{\text{Foss}}/a_E)$ in the ratio of the two airborne fractions. This ratio, $a_{\text{Foss}}/a_E = 1 + F_{\text{LUC}}/F_{\text{Foss}}$, decreased fairly steadily through 1959–2006 at a rate $r(a_{\text{Foss}}/a_E) \approx -0.4\% \text{ y}^{-1}$ (around an average a_{Foss}/a_E of 1.32) because F_{Foss} grew more quickly than F_{LUC} (Canadell et al., 2007). The decreasing trend in $F_{\text{LUC}}/F_{\text{Foss}}$ therefore accounts fully for the observed different signs in the growth rates of a_{Foss} and a_E .

Two further methodological checks were applied to all estimates of airborne-fraction growth rates. First, estimates of growth rates like $r(a_E)$ were found to have some sensitivity to the exact starting and ending times of the CO₂ series used to determine C'_a . The extent of this sensitivity was investigated with an enhanced stochastic trend estimation method, in which bootstrap subsampling of the time series under test was used to reduce sensitivity to starting and ending times (see Appendix C for details). Results from this method were statistically consistent with those given above, confirming the robustness of the estimated trends.

Second, the entire analysis was also carried out using individual-station CO₂ series from MLO and SPO instead of the globally-averaged series GLA and GLB. Results were similar to those with the globally-averaged series, despite the fact that [CO₂] at MLO was higher than at SPO by an offset which increased from ~ 1 ppm in the 1960s to ~ 3 ppm in 2000–2005. By using an exponential-growth model for C_a it can be shown that this offset accounts for a statistically insignificant difference in $r(a_E)$ of about $0.06\% \text{ y}^{-1}$.

4.3 Uncertainty in emissions from land use change

The largest uncertainty in the above results arises from F_{LUC} . The time series used here (Canadell et al., 2007) gives $F_{\text{LUC}} \approx 1.5 \text{ PgC y}^{-1}$ for the 1990s, with little change through the period 1959–2006. This is in the midrange of three existing estimates for the 1990s: 2.15 PgC y^{-1} (Houghton, 2003), 1.1 PgC y^{-1} (Achard et al., 2004) and 0.9 PgC y^{-1} (DeFries et al., 2002). The latter two values were based on remote-sensing estimates of cleared area, while the first was based on forest inventories and was subsequently revised downward to 1.5 PgC y^{-1} (Canadell et al., 2007). A recent satellite-based estimate of humid tropical forest clearing (Hansen et al., 2008) gives an area clearing rate similar to Achard et al. (2004) but no estimate of F_{LUC} . The large uncertainty in F_{LUC} originates from uncertainties in both cleared area and biomass (Houghton, 2005) and changes in inventory methodologies (Grainger, 2008).

Our estimated positive trend in airborne fraction ($r(a_E) \approx 0.24 \text{ y}^{-1}$) is reduced either if the mean value of F_{LUC} is proportionally revised downward, or if the trend in F_{LUC} is revised upward. Therefore, to assess the effect of possible uncertainties in F_{LUC} , we supplemented our primary calculation with two additional calculations using perturbed time series for F_{LUC} in directions which reduce the inferred airborne fraction trend. The first (“perturbation 1”) uses an F_{LUC} time series which is uniformly reduced to 0.6 of the primary values used here, giving values similar to the lowest estimate quoted above, 0.9 PgC y^{-1} for the 1990s (DeFries et al., 2002). The second (“perturbation 2”) assumes that the growth rate in FLUC is $1\% \text{ y}^{-1}$ higher than the time series used in the primary calculation, giving a perturbed F_{LUC} which is the same as the primary value in 2000 but 0.67 of the primary value in 1960.

Table 1. Mean values and proportional growth rates of airborne fraction (a_E), land fraction (l_E) and ocean fraction (o_E), from primary calculation and two perturbations to the time series for the net emission flux from land use change (F_{LUC}). In perturbation 1, F_{LUC} is reduced uniformly to 0.6 of its primary value. In perturbation 2, a 1% growth rate enhancement is applied to F_{LUC} by preserving the primary value in 2000 and reducing earlier estimates. Mean values are intercepts of linear trend lines in 1980. Proportional growth rates (in $\% \text{ y}^{-1}$) are given with 5% to 95% confidence intervals. Trends in brackets are not significantly different from zero (90% confidence level).

Quantity	Case	Mean	Growth rate ($\% \text{ y}^{-1}$)
Air (a_E)	Primary calculation	0.43	$+0.2 \pm 0.2$
Land (l_E)		0.27	$(+0.1 \pm 0.4)$
Ocean (o_E)		0.30	-0.4 ± 0.1
Air (a_E)	Perturbation 1: reduce F_{LUC}	0.47	$(+0.1 \pm 0.2)$
Land (l_E)		0.20	$+0.8 \pm 0.9$
Ocean (o_E)		0.33	-0.6 ± 0.1
Air (a_E)	Perturbation 2: increase $r(F_{\text{LUC}})$	0.45	(-0.0 ± 0.2)
Land (l_E)		0.24	$+0.9 \pm 0.4$
Ocean (o_E)		0.31	-0.7 ± 0.1

The effects of these perturbations are shown in Table 1. Perturbation 1 yields an estimated trend $r(a_E)$ in airborne fraction which is still positive but not significantly different from zero, while perturbation 2 yields nearly zero trend. However, both perturbations also have the effects of increasing the positive trend in the land fraction to values significantly above zero, and further decreasing the already negative trend in the ocean fraction. Both of perturbations 1 and 2 are near the edges of the present uncertainty bands around estimates of emissions from land use change. Opposite perturbations, which are also possible, would influence our primary trend estimates in the opposite sense and increase the estimated trend $r(a_E)$.

4.4 Implications

An increasing total airborne fraction implies that total sinks are increasing more slowly than total emissions, so that sinks are not keeping pace with emissions. This can be quantified by using Eq. (1) to write the relationship between the growth rate $r(-F_S)$ of total sinks and the growth rate $r(F_E)$ of total emissions, obtaining:

$$r(-F_S) = r(F_E) - \left(\frac{a_E}{1 - a_E} \right) r(a_E) \quad (11)$$

$$1.6 (\pm 0.2) \quad 1.8 (\pm < 0.1) \quad -0.2 (\pm 0.2)$$

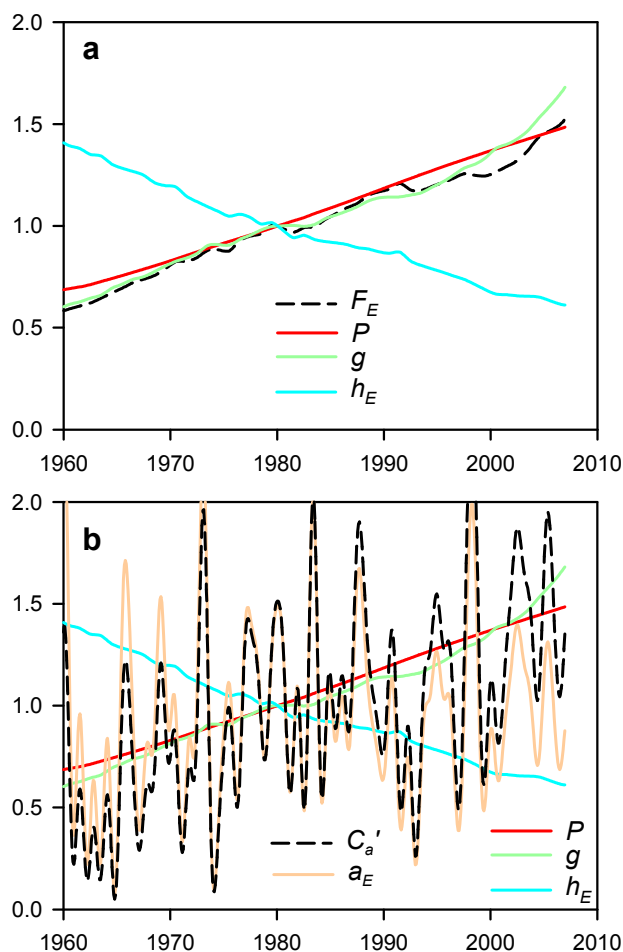


Fig. 6. (a) Factors in the Kaya identity, $F_E = Pgh_E$. The Kaya identity in this form expresses total emissions (F_E , dashed black) as the product of global population (P , red), per capita GDP-PPP (g , green) and the total carbon intensity of the global economy (h_E , blue). The carbon intensity h_E is the combined global CO₂ emission from fossil fuels and land use change per unit global GDP-PPP. (b) Factors in the extended Kaya identity, $C'_a = Pgh_E a_E$. This identity expresses the increase in the CO₂ growth rate (C'_a , dashed black) as the product of the Kaya factors P (red), g (green) and h_E (blue), together with the airborne fraction a_E (beige). In both panels, all factors are normalised to 1 in 1980.

The numbers beneath each term give average values and uncertainties in trends (in % y^{-1}) for 1959–2006. Sinks grew slightly slower than emissions, though both grew significantly.

The observed increase in the airborne fraction can be compared with available predictions from C⁴MIP, the Coupled Climate-Carbon Cycle Model Intercomparison Project (Friedlingstein et al., 2006). Eleven participating models gave scattered predictions for $r(a_E)$ for 1959–2006, averaging $r(a_E) = 0.27 \pm 0.36\% y^{-1}$ across all models and with 9 models predicting a negative trend, opposite in sign to the

observation. Equation (11) shows that this is a sensitive test for carbon-climate model predictions of trends in total sinks, because the sign of $r(a_E)$ is determined by the small difference between the two larger quantities $r(F_E)$ and $r(-F_S)$. Therefore, the fact that model predictions for $r(a_E)$ are not in agreement with each other or with observations is not an indication that all coupled carbon-climate model predictions should be dismissed.

5 Unified assessment of the drivers of CO₂ growth

To assess the relative effects on CO₂ growth of changes in airborne fraction and anthropogenic drivers of CO₂ emissions, we use an extended form of the Kaya identity. In its usual form (Nakicenovic et al., 2000; Nakicenovic, 2004; Raupach et al., 2007), the Kaya identity expresses global fossil-fuel CO₂ emissions as $F_{\text{Fossil}} = Pgef$, where P is global population, $g = G/P$ is per capita income or per capita GDP, $e = E/G$ is the energy intensity of GDP, $f = F_{\text{Fossil}}/E$ is the fossil-carbon intensity of energy, G is global GDP-PPP, and E is global primary energy consumption. An equivalent expression is $F_{\text{Fossil}} = Pgh_{\text{Fossil}}$, where $h_{\text{Fossil}} = F_{\text{Fossil}}/G = ef$ is the fossil-fuel carbon intensity of the global economy.

We modify this identity in two ways, first to describe total emissions ($F_E = F_{\text{Fossil}} + F_{\text{LUC}}$) rather than F_{Fossil} . Land use change emissions can be written in Kaya form as $F_{\text{LUC}} = Pgh_{\text{LUC}}$, where $h_{\text{LUC}} = F_{\text{LUC}}/G$ is the land-use-change carbon intensity of the global economy, corresponding to h_{Fossil} above. The Kaya identity for total CO₂ emissions is then

$$F_E = Pgh_{\text{Fossil}} + Pgh_{\text{LUC}} = Pgh_E \quad (12)$$

where $h_E = F_E/G = h_{\text{Fossil}} + h_{\text{LUC}}$ is the total carbon intensity of the global economy, accounting for both fossil fuels and land use change. Second, we describe the atmospheric CO₂ growth rate (C'_a) by introducing the airborne fraction $a_E = C'_a/F_E$ into Eq. (12), obtaining an extended Kaya identity in which a_E appears as an extra factor:

$$C'_a = Pgh_E a_E \quad (13)$$

The proportional growth rates of factors in Eqs. (12) and (13) are related by

$$\begin{aligned} r(F_E) &= r(P) + r(g) + r(h_E) \\ r(C'_a) &= r(P) + r(g) + r(h_E) + r(a_E) \end{aligned} \quad (14)$$

because $r(X) = X'/X$ yields $r(XYZ) = r(X) + r(Y) + r(Z)$ for any X , Y and Z . All terms in Eq. (14) have units time^{-1} . Note that $r(C'_a) = C''_a/C'_a$ is the proportional growth rate of the CO₂ growth rate, a measure of the second derivative of C_a .

Figures 6a and b respectively show time series of the factors in the Kaya identity for F_E , (Eq. 12) and the extended Kaya identity for C'_a (Eq. 13) for the period 1959–2006, with

Table 2. Proportional growth rates ($r(X)=X'/X$, in % y^{-1}) of factors in the Kaya identity ($F_E=gh_E$) and the extended Kaya identity ($C'_a=Pgh_Ea_E$), for periods 1959–2006, 1959–1999 and 2000–2006 (inclusive of end years). Errors denote approximate 5% to 95% confidence intervals. Where not shown, errors are less than $0.1\% y^{-1}$. Roundoff errors are responsible for slight departures from Eq. (14).

Period	1959–2006	1959–1999	2000–2006
$r(F_E)$	1.8	1.9	3.0
$r(P)$	1.7	1.7	1.2
$r(g)$	1.8	1.8	3.1 ± 0.1
$r(h_E)$	-1.7	-1.7	-1.2 ± 0.1
$r(a_E)$	0.2 ± 0.2	0.2 ± 0.3	0.2 ± 2.7
$r(C'_a)$	1.9 ± 0.3	1.9 ± 0.4	3.0 ± 2.7

series are normalised to 1 in 1980 so that trends can be compared. Figures 7a and b show the corresponding proportional growth rates (Eq. 14), with 7-year smoothing for clarity. Average growth rates of all factors, with 5% to 95% confidence intervals, are given in Table 2.

We first consider trends in total emissions (Figs. 6a and 7a). The average growth rate $r(F_E)$ over 1959–2006 was $1.8\% y^{-1}$, with interannual variability from less than 0.5 to over $3\% y^{-1}$. This growth was driven by additive contributions of $+1.7\% y^{-1}$ from $r(P)$ (growth in population), $+1.8\% y^{-1}$ from $r(g)$ (growth in income), and $-1.7\% y^{-1}$ from $r(h_E)$ (reduction or improvement in the total carbon intensity of the global economy). Uncertainties in all these growth rates are low ($0.1\% y^{-1}$ or less; Table 2).

There were significant interdecadal trends in the emissions drivers P , g and h_E through 1959–2006. Growth in population (P) slowed from 2 to $1.2\% y^{-1}$. Per capita income (g) grew more rapidly since 2000 than over the previous four decades, with $r(g)=3.0\% y^{-1}$ over 2000–2006 compared with $1.8\% y^{-1}$ over 1959–1999. Also, the negative growth rate (improvement) in the carbon intensity of the economy (h_E) declined since 2000: $r(h_E)$ was $-1.2\% y^{-1}$ over 2000–2006, compared with a mean of $-1.7\% y^{-1}$ over 1959–1999. (Figures for $r(h_E)$ differ from Canadell et al., 2007 for two reasons: the use of GDP-PPP here and GDP-MER (Market Exchange Rate) there, and the inclusion here of F_{LUC} in h_E). These trends have together driven a substantial recent increase in the growth rate of total emissions, with $r(F_E)=3.0\% y^{-1}$ over 2000–2006 compared with $1.9\% y^{-1}$ over 1959–1999. The growth rate in F_E ($=F_{Foss}+F_{LUC}$) is slightly lower than the recent growth rate in fossil-fuel emissions ($r(F_{Foss})=3.3\% y^{-1}$ over 2000–2006) because there has been no recent growth in the land-use-change emission (F_{LUC}).

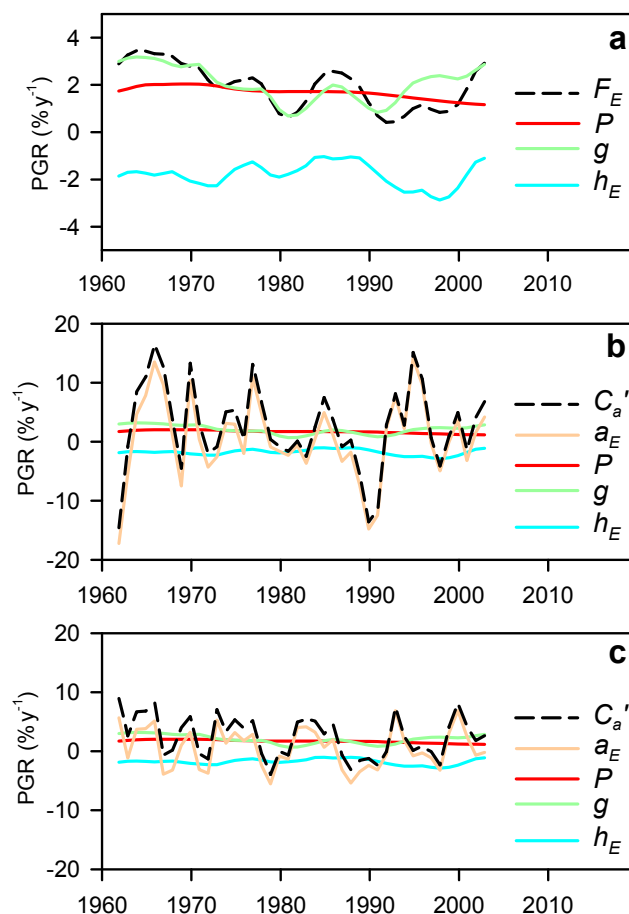


Fig. 7. (a) proportional growth rates ($\% y^{-1}$) of factors in the Kaya identity, $F_E=Pgh_E$; (b) growth rates of factors in the extended Kaya identity, $C'_a=Pgh_Ea_E$; (c) growth rates of factors in the noise-reduced version of the extended Kaya identity, $C'_a^{(n)}=Pgh_Ea_E^{(n)}$, where (n) denotes removal of the EVI-correlated fluctuating component. All growth rates are smoothed with a 7-year running mean. Colours match Fig. 6.

Trends in CO₂ growth rate (Figs. 6b and 7b) have more short-term variability. Beneath this variability C'_a has increased inexorably over the last five decades, reaching an average of $C'_a\approx 4.1\pm 0.1$ PgC y^{-1} or $[CO_2]'=1.9$ ppm y^{-1} through 2000–2006 (Canadell et al., 2007). Using Eq. (14), the drivers of this increase can be expressed as additive contributions from the growth rates $r(P)$, $r(g)$, $r(h_E)$ and $r(a_E)$ to $r(C'_a)=C'_a/C'_a$, the growth rate of the CO₂ growth rate. Even with the 7-year smoothing used here, $r(C'_a)$ fluctuated strongly around a mean of $+1.9\% y^{-1}$, with contributions from $r(P)$, $r(g)$, $r(h_E)$ and $r(a_E)$ given in Table 2. Averaged over the whole period 1959–2006, most of the interdecadal trend ($r(C'_a)\approx 1.9\% y^{-1}$) was attributable to increasing emissions ($r(F_E)\approx 1.8\% y^{-1}$), caused in turn by the growth rates of P , g and h_E . A small component of $r(C'_a)$, about $0.2\% y^{-1}$ out of $1.9\% y^{-1}$, was caused by the

interdecadal growth in airborne fraction, $r(a_E)$ (these figures do not satisfy Eq. (14) exactly because of statistical uncertainties and roundoff errors).

Most of the strong interannual variability in $r(C'_a)$ originates from variability in the CO₂ exchange flux F_S and thence the airborne fraction. Much of this variability in turn is associated with the EVI. Subtracting the EVI-correlated fluctuating component out of C'_a and a_E as in Sect. 4.2, we obtain a noise-reduced form of the extended Kaya identity, $C_a^{(n)} = Pgh_E a_E^{(n)}$. Figure 7c shows the growth rates of extended Kaya factors with this noise reduction. The variability in each of $r(C_a^{(n)})$ and $r(a_E^{(n)})$ is about half of the equivalent variability without noise reduction (Fig. 7b).

6 Discussion and conclusions

This paper has offered two main conclusions, the first being that the total airborne fraction is increasing at $r(a_E) \approx 0.2\% \text{ y}^{-1}$, with probability ≈ 0.9 of a positive trend. The immediate significance is that since 1959, growth in natural (land and ocean) sinks has fallen slightly behind growth in total (fossil plus land use change) emissions. This conclusion needs to be interpreted with regard for three factors: (1) there is uncertainty both from the statistics of interannual variability and also from imprecisely determined emissions from land use change; (2) the result does not imply that “sinks are weakening”, but rather shows that growth in sinks has not kept pace with growth in emissions; (3) the airborne fraction is a simple, robust diagnostic property of the carbon cycle which can provide the above conclusions but cannot partition trends in sinks between land and ocean – this requires additional information, supplied in Fig. 5 by modelled estimates of the ocean sink (Le Quéré et al., 2007).

The airborne fraction has another significance: it provides the gateway between the anthropogenic forcing and the atmospheric response of the carbon cycle. Total CO₂ emissions influence atmospheric CO₂ growth, and thence the CO₂ contribution to anthropogenic radiative forcing and climate change, via a set of carbon-cycle feedbacks with combined effects given by the airborne fraction. The relative roles of biophysical and anthropogenic influences can then be quantified by the extended Kaya identity, Eq. (13).

This leads to our second main conclusion: from 1959 to 2006, trends in anthropogenic factors (population, per-capita income and carbon intensity) have had a much greater effect on the growth rate of atmospheric CO₂ than the integrated trends in biophysical factors expressed by changes in the airborne fraction. The extended Kaya identity expresses the increase in the CO₂ growth rate ($1.9\% \text{ y}^{-1}$ over 1959–2006) as the sum of the growth rates of four global driving factors: population (P) contributed $+1.7\% \text{ y}^{-1}$; per capita income (g) contributed $+1.8\% \text{ y}^{-1}$; the total carbon intensity of the global economy (h_E) contributed $-1.7\% \text{ y}^{-1}$; and the airborne fraction (a_E) contributed $+0.2\% \text{ y}^{-1}$ with strong inter-

annual variability. The first three factors, the anthropogenic drivers, have therefore dominated the last, biophysical driver as contributors to accelerating CO₂ growth.

Further, the extended Kaya identity allows estimation of the relative impacts on future [CO₂] of likely future trends in all four drivers. To do this we consider the time interval Δt_x to reach a specified future “target” concentration [CO₂]_x at a given, steady $r(C'_a)$ (the growth rate of the CO₂ growth rate). The interval Δt_x can be determined analytically (Appendix D). We take the target [CO₂]_x = 450 ppm and initial conditions [CO₂] = 383 ppm and [CO₂]' = 2 ppm y⁻¹ in 2008. If $r(C'_a)$ continues at $2.0\% \text{ y}^{-1}$ (approximately the average for 1959–2006), then [CO₂] will reach 450 ppm in 26 years, in 2034. An increase in $r(C'_a)$ of $1\% \text{ y}^{-1}$, by any mechanism, shortens the time to reach 450 ppm by about 2.6 years. Since 2000, the combination of influences from the anthropogenic emissions drivers P , g and h_E have indeed increased $r(C'_a)$ by more than $1\% \text{ y}^{-1}$, as discussed above. For future growth in airborne fraction to have a comparable influence, $r(a_E)$ would need to increase several-fold from its 1959–2006 average of $0.2\% \text{ y}^{-1}$. This is well outside the range of predictions for $r(a_E)$ from C⁴MIP coupled carbon-climate model predictions for trends in airborne fraction through the 21st century (Friedlingstein et al., 2006).

To reduce emissions and thence atmospheric CO₂, it is necessary to reduce the growth rates of the emissions drivers P , g and h_E in some combination. Growth in population (P) is presently just over $1\% \text{ y}^{-1}$ and is forecast to decline to zero in the second half of the 21st century (Lutz et al., 2001). Growth in global per capita income (g) is needed to improve quality of life in the developing world. This leaves the primary option as increasing the negative growth rate in carbon intensity (h_E). To achieve a reduction rate in total emissions of $-2\% \text{ y}^{-1}$ (which would halve emissions in 35 years) in the presence of global growth rates of $2\% \text{ y}^{-1}$ in g and $1\% \text{ y}^{-1}$ in P , it is necessary to achieve a decline in h_E at a rate of around $-5\% \text{ y}^{-1}$, three times the 1959–2006 average. This highlights the significance of recent trends in emissions and carbon intensity.

Appendix A

Data sources and treatments

A1 CO₂ concentrations and growth rates

Four monthly CO₂ time series were used, denoted MLO, SPO, GLA and GLB. The first two were monthly time series for baseline [CO₂] at Mauna Loa (MLO, commencing March 1958) and the South Pole (SPO, commencing June 1957) from the Scripps Institution of Oceanography <http://scrippsco2.ucsd.edu/data/data.html> (Keeling et al., 2001, 2005). The versions of these series used here were gap-filled and had the quasi-regular annual cycle removed by

subtraction of a 4-harmonic fit with a linear gain factor. The monthly CO₂ growth rate with annual cycle removed was calculated from each series by a centred first difference. The third and fourth series were estimates of a globally averaged CO₂. The GLA series was formed from the average of MLO and SPO. The GLB series consisted of a globally-averaged CO₂ series available from January 1980 onward, augmented with MLO data for 1958–1979, with both series from the Earth Systems Research Laboratory of the National Oceanographic and Atmospheric Administration (NOAA-ESRL) <http://www.esrl.noaa.gov/gmd/ccgg/trends/>. The GLB series includes the annual cycle. Its trend is smooth but there is a discontinuity in the annual cycle at the join in 1980. The annual cycle was removed for determination of the trend in a_E .

A2 CO₂ emissions

The emissions datasets are identical to those in Canadell et al. (2007) and Raupach et al. (2007). Annual data on F_{FOSS} to 2004 are from the CDIAC (Marland and Rotty, 1984; Marland et al., 2006) <http://cdiac.ornl.gov/>, augmented by estimates for 2005 and 2006. Data on F_{LUC} are from Houghton (2003) as revised in Canadell et al. (2007). A monthly series for $F_E = F_{\text{FOSS}} + F_{\text{LUC}}$ for 1958 onward was constructed by spline interpolation of annual series for F_{FOSS} and F_{LUC} . It is likely that there are repeating annual cycles in both F_{FOSS} and F_{LUC} caused by seasonal patterns in energy consumption and land management practices, but interpolation of annual data gives a good approximation to monthly series with the annual cycle removed.

A3 ENSO indices

Five ENSO indices were used: Niño3, Niño3.4, Niño4, SOI, from <http://www.cpc.ncep.noaa.gov/data/indices/sstoi.indices>, and the MEI, from <http://www.cdc.noaa.gov/ClimateIndices/List/>. The MEI is constructed from the first principal components of sea-level pressure, zonal and meridional components of the surface wind, sea surface temperature, surface air temperature, and total sky cloudiness fraction (Wolter and Timlin, 1993, 1998).

A4 Volcanic aerosol index

VAI data in latitude bands (Ammann et al., 2003), to 1998, were obtained from ftp://ftp.ncdc.noaa.gov/pub/data/paleo/climate_forcing/volcanic_aerosols/ammann2003b_volcanics.txt. A global VAI was calculated by averaging with area weighting. The data were extended to 2006 assuming no volcanic activity between 1998 and 2006, consistent with Mishchenko et al. (2007).

A5 GDP-PPP and population

For 1970 and later, data sources are identical to those in Raupach et al. (2007). Global population (P) was from the United Nations Statistics Division <http://unstats.un.org/unsd/snaama/selectionbasicFast.asp>. Global GDP-PPP (G) was from the World Economic Outlook of the International Monetary Fund <http://www.imf.org/external/pubs/ft/weo/2006/02/data/download.aspx>. For times before 1970, both P and G were obtained from “Historical Statistics for the World Economy: 1-2003 AD” by Angus Maddison <http://www.ggdc.net/maddison/>. There was good agreement between these datasets in the overlap period 1970–2003.

Appendix B

Time series analysis

B1 Normalised cumulative spectra and cospectra

Let $X(t)$ and $Y(t)$ be continuous processes in time, or discrete time series, with zero mean. The normalised cumulative spectrum $\text{NC}_{[X,X]}(f)$ of $X(t)$ is the integral from 0 to f of the spectrum of the unit-variance process $X(t)/\sigma_X$ (where σ_X is the standard deviation of X); it is the fraction of the variance of X contributed by frequencies less than f . The normalised cumulative cospectrum $\text{NC}_{[X,Y]}(f)$ of $X(t)$ and $Y(t)$ is the integral from 0 to f of the cospectrum of the unit-variance processes $X(t)/\sigma_X$ and $Y(t)/\sigma_Y$; it is the fractional contribution to the XY covariance $\text{Cov}_{[X,Y]}$ from frequencies less than f , normalised so that $\text{NC}_{[X,Y]}(f)$ approaches the correlation coefficient $\text{Cov}_{[X,Y]} / (\sigma_X \sigma_Y)$ as $f \rightarrow \infty$.

B2 Fourier-transform lowpass filtering

The lowpass-filtered version of a series $X(t)$ was obtained by (a) taking the Fourier transform of $X(t)$; (b) setting Fourier components above the lowpass cutoff frequency to zero; (c) taking the inverse Fourier transform.

Appendix C

Trend estimation

The trend of a series $X(t)$ was estimated using a stochastic method as in (Le Quéré et al., 2007) and (Canadell et al., 2007), accounting for temporal correlation between data points. First, the trend X^T was found by conventional least-squares regression, yielding a trend line $X^T = x_0 + x_1 t$. The lagged autocorrelation function of the residual $(X - X^T)$ was fitted with an autoregressive (AR) model (Box et al., 1994) and used to generate an ensemble of 1000 stochastic realisations of the data with mean trend X^T and residuals correlated as in the data itself. The probability density function (PDF) of the slopes (x_1) in this ensemble was calculated, yielding trend statistics.

For supplementary investigation of the sensitivity of trends to the start and end points of the series $X(t)$, an “enhanced stochastic” method was used. This extends the stochastic method by taking the slope of the trend line X^T to be the mean of a 1000-member ensemble obtained by “bootstrap” (with replacement) sampling of subseries of $X(t)$ with random starting and stopping times (t_0, t_1) , such that $(t_1 - t_0)$ is at least a minimum fraction f_{\min} of the total duration of the data series $X(t)$. We took $f_{\min} = 0.8$. The statistics of this ensemble are similar to those of the original series $X(t)$, with sensitivity to choice of t_0 and t_1 reduced by averaging over many realisations.

Appendix D

Time to reach a specified CO₂ concentration

We seek the time interval Δt_x to reach a specified future concentration $[\text{CO}_2]_x$, with a given steady growth rate of the CO₂ growth rate, $r_C = r(C'_a)$, and given initial concentration $[\text{CO}_2]_0$ and rate of increase $[\text{CO}_2]'_0$ at time t_0 . Thus $r_C = [\text{CO}_2]''_0 / [\text{CO}_2]'_0$, and is held steady. The equation governing $[\text{CO}_2](t)$ is

$$[\text{CO}_2]'' = r_C [\text{CO}_2]' \quad (\text{D1})$$

and the resulting CO₂ trajectory is

$$[\text{CO}_2](t) = [\text{CO}_2]_0 + \frac{[\text{CO}_2]'_0}{r_C} \exp(r_C(t - t_0) - 1) \quad (\text{D2})$$

At a given r_C , the time to reach $[\text{CO}_2]_x$ is

$$\Delta t_x = \frac{1}{r_C} \ln(r_C T - 1) \quad (\text{D3})$$

where $T = ([\text{CO}_2]_x - [\text{CO}_2]_0) / [\text{CO}_2]'_0$ is a time scale. Physiologically, T is the time to reach $[\text{CO}_2]_x$ when the rate of increase in $[\text{CO}_2]$ is held steady at its initial value $[\text{CO}_2]'_0$. If $r_C > 0$, then Δt_x is less than T . In the limit $r_C \rightarrow 0$, Δt_x approaches T .

Acknowledgements. This work was undertaken by the Global Carbon Project (GCP, www.globalcarbonproject.org) of the Earth System Science Partnership (www.essp.org). Support for the GCP from the Australian Climate Change Science Program is acknowledged with appreciation. We gratefully acknowledge the teams from both the Scripps Institution of Oceanography and NOAA-ESRL, who have publicly released the CO₂ records without which this work would not have been possible. We thank P. Briggs for help with preparation of figures.

Edited by: C. Heinze

References

- Achard, F., Eva, H. D., Mayaux, P., Stibig, H. J., and Belward, A.: Improved estimates of net carbon emissions from land cover change in the tropics for the 1990s, *Global Biogeochem. Cy.*, 18, GB2008.1–GB2008.11, doi:10.1029/2003GB002142, 2004.
- Ammann, C. M., Meehl, G. A., Washington, W. M., and Zender, C. S.: A monthly and latitudinally varying volcanic forcing dataset in simulations of 20th century climate, *Geophys. Res. Lett.*, 30, 1657, doi:10.1029/2003GL016875, 2003.
- Box, G., Jenkins, G. M., and Reinsel, G.: *Time series analysis: forecasting and control*, 3rd edition, Prentice Hall, Englewood Cliffs, NJ, USA, 592 pp., 1994.
- Canadell, J. G., Le Quééré, C., Raupach, M. R., Field, C. B., Buitenhuis, E. T., Ciais, P., Conway, T. J., Gillett, N. P., Houghton, R. A., and Marland, G.: Contributions to accelerating atmospheric CO₂ growth from economic activity, carbon intensity, and efficiency of natural sinks, *PNAS*, 0702737104, 104, 18 866–18 870, 2007.
- DeFries, R. S., Houghton, R. A., Hansen, M. C., Field, C. B., Skole, D., and Townshend, J.: Carbon emissions from tropical deforestation and regrowth based on satellite observations for the 1980s and 1990s, *PNAS*, 99, 14 256–14 261, 2002.
- Enting, I. G.: Laplace transform analysis of the carbon cycle, *Environ. Model. Software*, 22, 1488–1497, 2007.
- Friedlingstein, P., Cox, P., Betts, R., Bopp, L., von Bloh, W., Brovkin, V., Cadule, P., Doney, S., Eby, M., Fung, I., Bala, G., John, J., Jones, C., Joos, F., Kato, T., Kawamiya, M., Knorr, W., Lindsay, K., Matthews, H. D., Raddatz, T., Rayner, P., Rieck, C., Roeckner, E., Schnitzler, K. G., Schnur, R., Strassmann, K., Weaver, A. J., Yoshikawa, C., and Zeng, N.: Climate-carbon cycle feedback analysis: Results from the C4MIP model inter-comparison, *J. Clim.*, 19, 3337–3353, 2006.
- Grainger, A.: Difficulties in tracking the long-term global trend in tropical forest area, *PNAS*, 105, 818–823, 2008.
- Gruber, N., Friedlingstein, P., Field, C. B., Valentini, R., Heimann, M., Richey, J. D., Romero Lankao, P., Schulze, E.-D., and Chen, C.-T. A.: The vulnerability of the carbon cycle in the 21st century: an assessment of carbon-climate-human interactions, in: *The Global Carbon Cycle: integrating humans, climate, and the natural world*, edited by: Field, C. B. and Raupach, M. R., Island Press, Washington, USA, 45–76, 2004.
- Gu, L. H., Baldocchi, D. D., Wofsy, S. C., Munger, J. W., Michalsky, J. J., Urbanski, S. P., and Boden, T. A.: Response of a deciduous forest to the Mount Pinatubo eruption: enhanced photosynthesis, *Science*, 299, 2035–2038, 2003.
- Hansen, M. C., Stehman, S. V., Potapov, P. V., Loveland, T. R., Townshend, J. R. G., DeFries, R. S., Pittman, K. W., Arunarwati, B., Stolle, F., Steininger, M. K., Carroll, M., and DiMiceli, C.: Humid tropical forest clearing from 2000 to 2005 quantified by using multitemporal and multiresolution remotely sensed data, *PNAS*, 105, 9439–9444, 2008.
- Houghton, R. A.: Revised estimates of the annual net flux of carbon to the atmosphere from changes in land use and land management 1850–2000, *Tellus*, 55B, 378–390, 2003.
- Houghton, R. A.: Aboveground forest biomass and the global carbon balance, *Global Change Biol.*, 11, 945–958, 2005.
- Jones, C. D., Collins, M., Cox, P. M., and Spall, S. A.: The carbon cycle response to ENSO: a coupled climate-carbon cycle model study, *J. Clim.*, 14, 4113–4129, 2001.

- Jones, C. D. and Cox, P. M.: Modeling the volcanic signal in the atmospheric CO₂ record, *Global Biogeochem. Cy.*, 15, 453–465, 2001.
- Jones, C. D. and Cox, P. M.: On the significance of atmospheric CO₂ growth rate anomalies in 2002–2003, *Geophys. Res. Lett.*, 32, L14816, doi:10.1029/2005GL023027, 2005.
- Keeling, C. D. and Revelle, R.: Effects of El-Niño southern oscillation on the atmospheric content of carbon-dioxide, *Meteoritics*, 20, 437–450, 1985.
- Keeling, C. D., Whorf, T. P., Wahlen, M., and Vanderpligt, J.: Interannual extremes in the rate of rise of atmospheric carbon-dioxide since 1980, *Nature*, 375, 666–670, 1995.
- Keeling, C. D., Piper, S. C., Bacastow, R. B., Wahlen, M., Whorf, T. P., Heimann, M., and Meijer, H. A.: Exchanges of atmospheric CO₂ and ¹³CO₂ with the terrestrial biosphere and oceans from 1978 to 2000: 1. global aspects, *SIO Reference Series*, 01–06, Scripps Institution of Oceanography, San Diego, USA, 88, 2001.
- Keeling, C. D., Piper, S. C., Bacastow, R. B., Wahlen, M., Whorf, T. P., Heimann, M., and Meijer, H. A.: Atmospheric CO₂ and ¹³CO₂ exchange with the terrestrial biosphere and oceans from 1978 to 2000: observations and carbon cycle implications, in: *A history of atmospheric CO₂ and its effects on plants, animals, and ecosystems*, edited by: Ehleringer, J. R., Cerling, T. E., and Dearing, M. D., Springer Verlag, New York, USA, 83–113, 2005.
- Knorr, W., Scholze, M., Gobron, N., Pinty, B., and Kaminski, T.: Global-scale drought caused atmospheric CO₂ increase, *EOS*, 86, 178–181, 2005.
- Le Quéré, C., Rodenbeck, C., Buitenhuis, E. T., Conway, T. J., Langenfelds, R., Gomez, A., Labuschagne, C., Ramonet, M., Nakazawa, T., Metzl, N., Gillett, N., and Heimann, M.: Saturation of the southern ocean CO₂ sink due to recent climate change, *Science*, 316, 1735–1738, 2007.
- Lutz, W., Sanderson, W., and Scherbov, S.: The end of world population growth, *Nature*, 412, 543–545, 2001.
- Marland, G., Boden, T. A., and Andres, R. J.: Global, regional, and national CO₂ emissions, in: *Trends: a compendium of data on global change*, Carbon Dioxide Information Analysis Center, Oak Ridge National Laboratory, US Department of Energy, Oak Ridge, Tennessee, USA, available online: <http://cdiac.ornl.gov>, 2006.
- Marland, G. and Rotty, R. M.: Carbon dioxide emissions from fossil fuels: a procedure for estimation and results for 1950–82, *Tellus B*, 36, 232–261, 1984.
- Mishchenko, M. I., Geogdzhayev, I. V., Rossow, W. B., Cairns, B., Carlson, B. E., Laci, A. A., Liu, L., and Travis, L. D.: Long-term satellite record reveals likely recent aerosol trend, *Science*, 315, 1543, 2007.
- Nakicenovic, N.: Socioeconomic driving forces of emissions scenarios, in: *The Global Carbon Cycle: integrating humans, climate, and the natural world*, edited by: Field, C. B. and Raupach, M. R., Island Press, Washington, 225–239, 2004.
- Nakicenovic, N., Alcamo, J., Davis, G., de Vries, B., Fenhann, J., Gaffin, S., Gregory, K., Grubler, A., Jung, T. Y., Kram, T., La Rovere, E. L., Michaelis, L., Mori, S., Morita, T., Pepper, W., Pitcher, H., Price, L., Raihi, K., Roehrl, A., Rogner, H.-H., Sankovski, A., Schlesinger, M., Shukla, P., Smith, S., Swart, R., van Rooijen, S., Victor, N., and Dadi, Z.: *IPCC Special Report on Emissions Scenarios*, Cambridge University Press, Cambridge, UK, and New York, USA, 599 pp., 2000.
- Oeschger, H., Siegenthaler, U., and Heimann, M.: The carbon cycle and its perturbations by man, in: *Interactions of Energy and Climate*, edited by: Bach, W., Pankrath, J., and Williams, J., Reidel, Dordrecht, The Netherlands, 107–127, 1980.
- Raupach, M. R., Marland, G., Ciais, P., Le Quéré, C., Canadell, J. G., Klepper, G., and Field, C. B.: Global and regional drivers of accelerating CO₂ emissions, *PNAS*, 0700609104, 104, 10288–10293, 2007.
- Sabine, C. L., Heimann, M., Artaxo, P., Bakker, D. C. E., Chen, C.-T. A., Field, C. B., Gruber, N., Le Quéré, C., Prinn, R. G., Richey, J. D., Romero Lankao, P., Sathaye, J. A., and Valentini, R.: Current status and past trends of the global carbon cycle, in: *The global carbon cycle: integrating humans, climate, and the natural world*, edited by: Field, C. B. and Raupach, M. R., Island Press, Washington, USA, 17–44, 2004.
- Wolter, K. and Timlin, M. S.: Monitoring ENSO in COADS with a seasonally adjusted principal component index, in: *Proceedings of the 17th Climate Diagnostics Workshop*, Oklahoma Climatological Survey, Cooperative Institute for Mesoscale Meteorological Studies, and the School of Meteorology, University of Oklahoma, Norman, OK, USA, 52–57, 1993.
- Wolter, K. and Timlin, M. S.: Measuring the strength of ENSO – how does 1997/98 rank?, *Weather*, 53, 315–324, 1998.
- Zeng, N., Mariotti, A., and Wetzel, P.: Terrestrial mechanisms of interannual CO₂ variability, *Global Biogeochem. Cy.*, 19, GB1016, doi:10.1029/2004GB002273, 2005.